JACS
JOURNAL OF THE AMERICAN CHEMICAL SOCIETY

Communication

pubs.acs.org/JACS

π-Conjugated Nickel Bis(dithiolene) Complex Nanosheet

Tetsuya Kambe,[†] Ryota Sakamoto,[†] Ken Hoshiko,[†] Kenji Takada,[†] Mariko Miyachi,[†] Ji-Heun Ryu,[‡] Sono Sasaki,[§,∥] Jungeun Kim,[∥] Kazuo Nakazato,[‡] Masaki Takata,[∥,⊥] and Hiroshi Nishihara*[,†]

[†]Department of Chemistry, Graduate School of Science, The University of Tokyo, 7-3-1 Hongo, Bunkyo-ku, Tokyo 113-0033, Japan

[‡]Department of Electrical Engineering and Computer Science, School of Engineering, Nagoya University, Furo-cho, Chikusa-ku, Nagoya 464-8603, Japan

[§]Department of Biobased Materials Science, Graduate School of Science and Technology, Kyoto Institute of Technology, Hashigami-cho, Matsugasaki, Sakyou-ku, Kyoto 606-8585, Japan

[∥]Japan Synchrotron Radiation Research Institute (JASRI)/SPring-8, 1-1-1 Kouto, Sayo-cho, Sayo-gun, Hyogo 679-5198, Japan

[⊥]SPring-8 Center, RIKEN, 1-1-1 Kouto, Sayo-cho, Sayo-gun, Hyogo 679-5148, Japan

Supporting Information

ABSTRACT: A π-conjugated nanosheet comprising planar nickel bis(dithiolene) complexes was synthesized by a bottom-up method. A liquid−liquid interfacial reaction using benzenehexathiol in the organic phase and nickel(II) acetate in the aqueous phase produced a semiconducting bulk material with a thickness of several micrometers. Powder X-ray diffraction analysis revealed that the crystalline portion of the bulk material comprised a staggered stack of nanosheets. A single-layer nanosheet was successfully realized using a gas−liquid interfacial reaction. Atomic force microscopy and scanning tunneling microscopy confirmed that the π-conjugated nanosheet was single-layered. Modulation of the oxidation state of the nanosheet was possible using chemical redox reactions.

Monolayer nanosheet materials have attracted significant attention because of their unique physical and chemical properties, which derive from their two-dimensional (2D) nature. Graphene is one of the most prominent nanosheet materials because of its various attractive properties, including high carrier mobilities.[1] Graphene is being utilized in electronics,[1−3] photonics,[4] and spintronics[5,6] applications. The anticipated practical success of graphene has prompted researchers to investigate other types of 2D nanosheets, including metal oxides,[7−11] metal sulfides,[12−15] metal hydroxides,[16−20] and silicon nanosheets.[21−23] These materials also possess various interesting and useful properties, including semiconductivity,[10,15] ferroelectricity,[8,14] and photoluminescence.[9,19−22] Most of the nanosheets listed above have been synthesized via exfoliation of bulk layered materials, which is a top-down method.

Recently, the bottom-up synthesis of nanosheets has been extensively investigated. The advantages of bottom-up approaches are substantial. First, the composition, structure, and various properties can be tuned at will by tailoring the utilized components (e.g., the metal ion and ligand molecules or boronic acid and catecholic substances). Second, and importantly, the nanosheets that can be produced are not limited to the layers of bulk materials. Therefore, bottom-up synthesis may broaden the diversity and utility of nanosheets. Examples of this include surface metal−organic frameworks (surMOFs),[24] surface covalent-organic frameworks (surCOFs),[25,26] and bis(terpyridine)−metal complex nanosheets.[27] One of the unexplored potentialities of bottom-up processes is that a highly π-conjugated framework like graphene has not been realized. A further significant virtue of the bottom-up nanosheet is that its physical properties may be controlled by the switching behavior of its molecular components (e.g., redox, photoisomerization, and spin crossover). Molecular switching in the bottom-up nanosheet, however, is yet to be demonstrated.

Motivated by these considerations, we synthesized π-conjugated nanosheet **1** comprising nickel bis(dithiolene) units (Figure 1). This was achieved through a coordination reaction between benzenehexathiol (BHT) and nickel(II) acetate [Ni(OAc)$_2$]. BHT acts as a multichelating ligand extending in the equilateral-triangular direction. Metalladithiolene chemistry has revealed that d^8 metal ions of group 10 prefer the square-planar

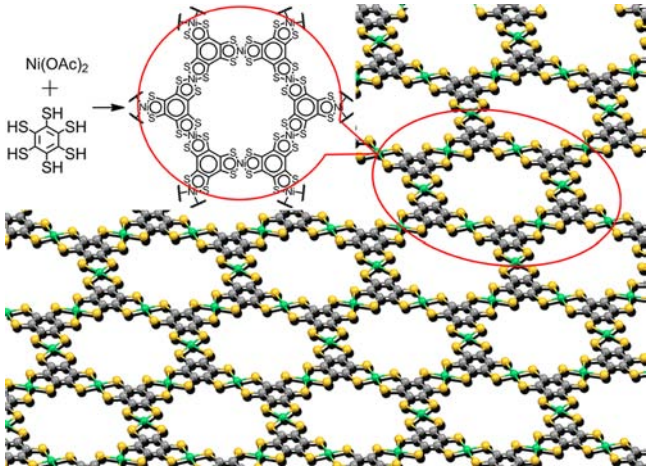

Figure 1. Schematic illustration and chemical structure of monolayer nickel bis(dithiolene) complex nanosheet **1**. Countercations have been omitted for clarity. Gray, C; yellow, S; green, Ni.

Received: December 19, 2012
Published: January 29, 2013

   dx.doi.org/10.1021/ja312380b | J. Am. Chem. Soc. 2013, 135, 2462−2465

coordination mode.[28] We expected that these characteristics of the components would produce a 2D planar nanosheet with sixfold symmetry via the formation of the nickel bis(dithiolene) motif. We note that **1** was conceived from our previous research on trinuclear metalladithiolene complexes and cluster complexes produced using BHT.[29−31] These complexes exhibited strong charge delocalization among the three metalladithiolene units through the phenylene linker in mixed-valent (MV) states. As a result of the intense communication between the π orbitals of the two metalladithiolene rings in metal bis(dithiolene) complexes,[32,33] **1** was expected to feature highly developed π conjugation. In addition, the nickel bis(dithiolene) complex shows reversible redox behavior (0, −1, and −2 are possible oxidation states).[33] We expected that redox switching would also be possible in nanosheet **1**.

First, we attempted the liquid−liquid interfacial synthesis of a nickel bis(dithiolene) nanosheet (Figure 2a). The aqueous phase

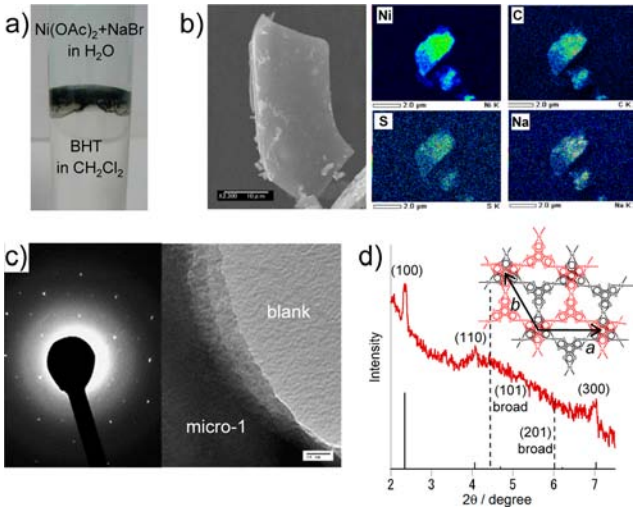

Figure 2. Synthesis and characterization of **micro-1**. (a) Photograph focusing on the water−CH_2Cl_2 interface holding **micro-1**. (b) (left) FE-SEM image and (right) elemental mapping of Ni, S, C, and Na performed using SEM−EDS. (c) (left) SAED pattern and (right) HRTEM image. (d) Experimental (red curve) and simulated (black sticks) PXRD patterns. See Figure S3 for details of the simulation.

included $Ni(OAc)_2$ (5 mM) along with NaBr (1 mM) as the source of a charge-compensating countercation (Na^+), and the organic (CH_2Cl_2) layer contained BHT (0.24 mM). The organic layer was initially overlaid with pure water, and an aqueous solution of $Ni(OAc)_2$ and NaBr was then gently added to the pure water layer, thus allowing a calm liquid−liquid interface to be maintained. When placed in an Ar atmosphere for 1 day, the material became a black solid with a metallic luster at the interface (denoted henceforth as **micro-1**; Figure 2a). In any solvent, **micro-1** was found to be absolutely insoluble. After the material was thoroughly washed with pure solvents (water, ethanol, and CH_2Cl_2) and dried under vacuum at 150 °C, various analyses were performed.

Figure 2b,c shows field-emission scanning electron microscopy (FE-SEM) and high-resolution transmission electron microscopy (HR-TEM) images of **micro-1**. The former shows **micro-1** to be monolithic with a lateral size of ∼100 μm and a thickness of 1−2 μm. SEM−energy dispersive spectroscopy (SEM−EDS) was conducted at the same time (Figure 2b). Elemental mapping indicated uniform distribution of each element (Ni, S, C, and Na), confirming the compositional homogeneity of **micro-1**. HR-TEM displayed a stairlike morphology at the edge of **micro-1**, indicative of a layered structure. Furthermore, selected-area electron diffraction (SAED) showed a hexagonal diffraction pattern [Figure 2c and Figure S1 in the Supporting Information (SI)], implying the formation of a hexagonal lattice with a cell length of 1.4−1.5 nm.

Figure S2 shows attenuated total reflection IR (ATR-IR) spectra of **micro-1** and BHT as a reference. BHT featured a strong signal at ∼2500 cm^{-1} that can be ascribed to the S−H stretching vibration. The peak disappeared completely in **micro-1**. Instead, C−$S^\bullet$ stretching peaks emerged at 1021 and 1084 cm^{-1}, indicating that all of the thiol groups of BHT participated in coordinating to the Ni ions to form the nickel bis(dithiolene) motif.[34]

Powder X-ray diffraction (PXRD) analysis of **micro-1** using high-energy synchrotron radiation produced several diffraction peaks (Figure 2d). This diffraction pattern was reproduced using a crystal model with the $P6_3/mmc$ space group with $a = b = 1.41$ nm and $c = 0.76$ nm (Figures 2d and S3). The a and b axes are identical to the in-plane periodicity of the nanosheet. On the other hand, the c axis is perpendicular to the nanosheet: The nanosheet layers stack in a staggered fashion. The sharp (100), (110), and (300) diffraction peaks were associated with the in-plane periodicity. In contrast, the (101) and (201) diffraction peaks involving in the out-of-plane periodicity were broad. PXRD indicated that a part of **micro-1** was in a crystalline state.

Electrochemical measurements disclosed the redox activity of **micro-1** (Figure 3a). One reversible redox wave derived from the

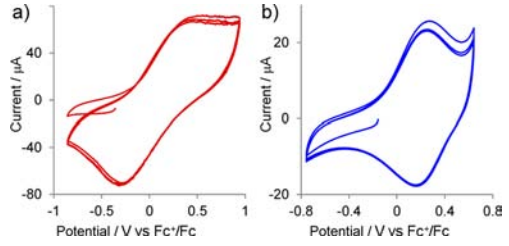

Figure 3. Cyclic voltammograms of (a) **micro-1** on glassy carbon in 0.1 M Bu_4NPF_6/CH_2Cl_2 and (b) **nano-1** on HOPG in 1 M Bu_4NClO_4/CH_2Cl_2.

0/−1 redox couple was observed at 0.05 V vs ferrocenium/ferrocene (Fc^+/Fc). The −1/−2 redox couple was not observed in the available potential window.

X-ray photoelectron spectroscopy (XPS) of **micro-1** on highly oriented pyrolytic graphite (HOPG) revealed the existence of Ni, S, and Na (Figure S4). This analysis also disclosed the oxidation state of the nickel bis(dithiolene) unit, which is strongly reflected in the binding energy of the S atom.[35] Deconvolution of the S 2s peak revealed that the nickel bis(dithiolene) moieties of **micro-1** took MV states comprising the 0 and −1 oxidation states in a 26:74 ratio (Figure S5).

It is worth noting that the oxidation state of **micro-1** could be changed by a chemical redox reaction. Treatment of **micro-1** with 7,7,8,8-tetracyanoquinodimethane radical anion sodium salt (NaTCNQ) [$E^{0\prime}$(TCNQ/$TCNQ^-$) = −0.30 V][36] gave rise to **reduced micro-1**, in which all of the nickel bis(dithiolene) units are in the −1 oxidation state. The occurrence of reduction was demonstrated using ATR-IR (Figure 4a) and XPS (Figure 4b). As-prepared **micro-1** featured two peaks at 1021 and 1084 cm^{-1} (Figure 4a). A mononuclear nickel bis(dithiolene) complex in

dx.doi.org/10.1021/ja312380b | J. Am. Chem. Soc. 2013, 135, 2462−2465

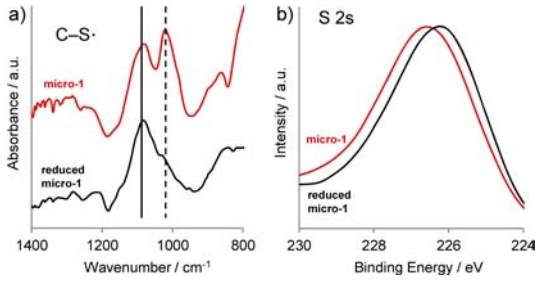

Figure 4. Determination of the oxidation state of **micro-1** before and after chemical reduction: (a) ATR-IR and (b) S 2s XPS of as-prepared **micro-1** (red) and **reduced micro-1** (black).

the −1 oxidation state features a C−S$^{\bullet}$ stretching mode at 1114 cm^{-1}, which splits into two bands at 1029 and 1099 cm^{-1} in the 0 oxidation state.[34] In reference to the mononuclear complex, the C−S$^{\bullet}$ stretching bands in as-prepared **micro-1** were assigned as follows: The 0 oxidation state contributes solely to the absorption at 1021 cm^{-1}, whereas that at 1084 cm^{-1} comprises the C−S$^{\bullet}$ stretching modes of both the 0 and −1 oxidation states. In **reduced micro-1**, the peak at 1021 cm^{-1} was lost, indicating that the nickel bis(dithiolene) units in the 0 oxidation state were reduced to the −1 state. The S 2s peak in the XPS spectrum of **reduced micro-1** possessed a lower binding energy (226.2 eV) than as-prepared **micro-1** (226.6 eV). A similar decrease in the binding energy upon reduction ascribable to the accumulation of negative charges at the sulfur atoms was observed in a mononuclear nickel bis(dithiolene) complex (Table S1 in the SI). Peak deconvolution indicated that all of the nickel bis(dithiolene) units were reduced to the −1 oxidation state (Figure S5). These results show that the oxidation state of **micro-1** can be modulated using chemical redox reactions.

The electrical conductivities of pelletized as-prepared **micro-1** and **reduced micro-1** were measured using a two-electrode configuration (Figure S6). As-prepared **micro-1** gave a conductivity of 0.15 S cm^{-1} at 298 K. On the other hand, **reduced micro-1** had a much lower conductivity of 6.7×10^{-3} S cm^{-1} at the same temperature. As demonstrated using ATR-IR and XPS, as-prepared **micro-1** possessed an 0/−1 MV oxidation state, whereas all of the nickel bis(dithiolene) units in **reduced micro-1** were in the −1 oxidation state. The difference in the conductivities indicates that the MV state contributes to the higher conductivity of as-prepared **micro-1** relative to the reduced one and that the oxidation state can be successfully modulated upon chemical reduction.

To produce single-layer or few-layer **1** (denoted hereafter as **nano-1**), we used a gas−liquid interfacial reaction (Figure 5a). An ethyl acetate solution (190 μL) of BHT (35 μM) was gently sparged onto the surface (77.5 cm^2) of an aqueous solution of $Ni(OAc)_2$ (50 mM) and NaBr (10 mM) using a microsyringe. The amount of BHT was restricted such that BHT covered only half of the aqueous surface. The reaction system was matured for 2 h in an Ar atmosphere, during which time the ethyl acetate evaporated spontaneously, and the resultant **nano-1** remaining at the gas−liquid interface was then salvaged onto HOPG.

Scanning probe microscopy (SPM) measurements were used to determine the structure of **nano-1** (Figure 5b−e). Its structure could be clearly distinguished from the bare HOPG surface in an atomic force microscopy (AFM) phase image (greater by 4°; Figure 5b). On the other hand, the AFM topological image of **nano-1** showed a smooth surface, and the cross-sectional analysis revealed a thickness of 0.6 nm (Figure 5c). This value is feasible

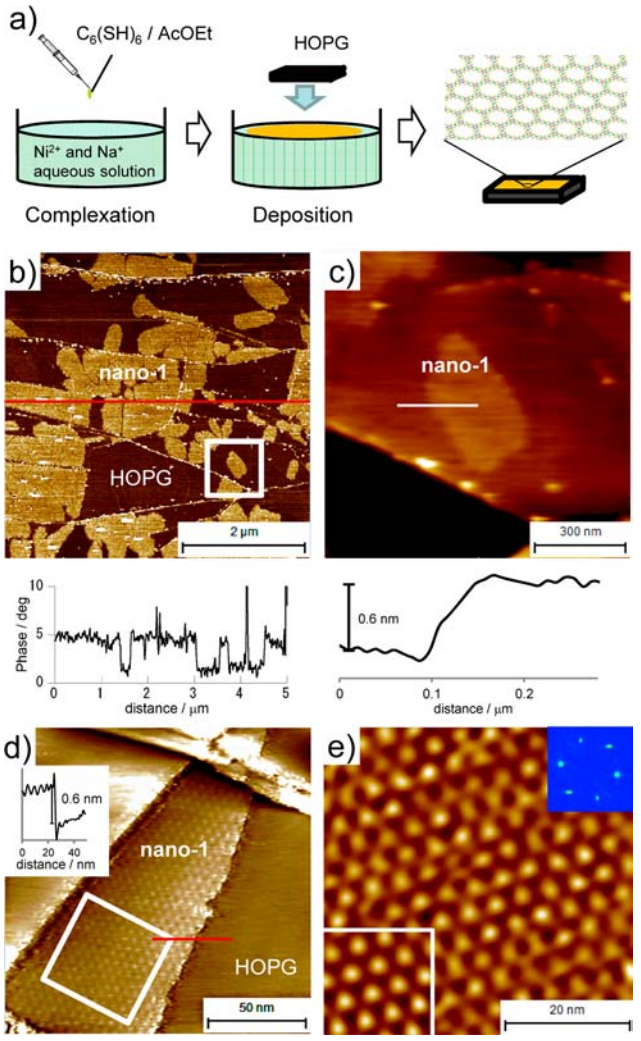

Figure 5. Synthesis and characterization of **nano-1**. (a) Illustration of the synthesis of **nano-1**. (b) (top) AFM phase image on HOPG and (bottom) its cross-sectional analysis. The bright areas correspond to **nano-1**. (c) (top) AFM topological image of single-layer **nano-1** and (bottom) and its cross-sectional analysis. The white square in (b) corresponds to the scan area. (d) STM topological image of single-layer **nano-1** on HOPG. The inset shows a cross-sectional analysis. The hexagonal structure is a moiré interference pattern composed of single-layer **nano-1** and HOPG substrate. (e) Close-up of the hexagonal pattern shown in the white square in (d). The upper-right and lower-left insets are the fast Fourier transform (FFT) of the STM image and the FFT-filtered image, respectively.

for a single-layer nanosheet, as AFM measurements of monolayer graphene on Si/SiO_2 substrates give a thickness of 0.5−1.0 nm depending on the interaction between graphene and the substrate.[1,37] A scanning tunneling microscopy (STM) image of **nano-1** showed a hexagonal pattern with a height of 0.6 nm (Figure 5d,e). The periodicity of the hexagonal pattern (4.90 nm) was too large to be assigned directly to the in-plane lattice of **nano-1** (1.41 nm from PXRD for **micro-1**). Instead, we ascribe it to a moiré pattern composed of **nano-1** and HOPG with a relative orientation angle of 1.4° (Figure S7).

The cyclic voltammogram of **nano-1** on HOPG is shown in Figure 3b. A reversible redox wave was observed at 0.21 V vs Fc^+/Fc, which we ascribe to the 0/−1 redox couple of the nickel bis(dithiolene) unit.

dx.doi.org/10.1021/ja312380b | J. Am. Chem. Soc. 2013, 135, 2462−2465

XPS of **nano-1** on HOPG detected the constitutive elements (S, Ni, and Na; Figure S8). The oxidation state of the nickel bis(dithiolene) unit was determined to be a mixture of 0 and −1 in a 63:37 ratio (Figure S9). As with **micro-1**, the oxidation state of **nano-1** could be tuned by chemical reduction using NaTCNQ. In this case, the reductant was added to the synthetic mixture, so **reduced nano-1** was obtained. The S 2s XPS signal of **reduced nano-1** underwent a decrease in the binding energy (Figure 6). Peak deconvolution suggested that all of the nickel bis(dithiolene) units were reduced to the −1 state (Figure S9).

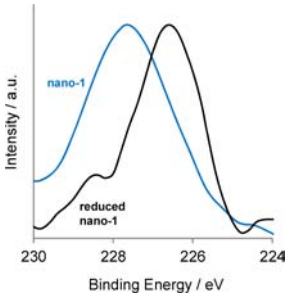

Figure 6. S 2s XPS spectra of **nano-1** and **reduced nano-1**.

In conclusion, we synthesized a π-conjugated nickel bis(dithiolene) nanosheet. Liquid−liquid and gas−liquid interface reactions using BHT and $Ni(OAc)_2$ were used to realize regulated coordination between the two components, which produced micrometer-thick **micro-1** and nanometer-thick **nano-1**, respectively. The crystalline structure, composition, and properties of **micro-1** were comprehensively identified using PXRD, XPS, SEM, HR-TEM, IR spectroscopy, elemental analysis, and electrochemical measurements. **micro-1** was shown to be semiconducting. SPM measurements revealed that **nano-1** features a hexagonally ordered monolayer structure. The redox states of both **micro-1** and **nano-1** can be switched by means of chemical reduction with NaTCNQ. Our successful fabrication of π-conjugated nanosheet **1** by means of the bottom-up coordination method represents an advance in nanosheet chemistry and could lead to applications in molecular electronics and materials.

■ ASSOCIATED CONTENT

Ⓢ Supporting Information

Experimental methods; TEM, SAED, ATR-IR, PXRD, XPS, and electrical conductivity data; analysis of the moiré pattern of **nano-1** on HOPG; and complete ref 12. This material is available free of charge via the Internet at http://pubs.acs.org.

■ AUTHOR INFORMATION

Corresponding Author

nisihara@chem.s.u-tokyo.ac.jp

Notes

The authors declare no competing financial interest.

■ ACKNOWLEDGMENTS

The authors acknowledge Grants-in-Aid from MEXT of Japan (24750054 and 21108002, Area 2107, Coordination Programming) and a Research Fellowship for Young Scientists from JSPS. The synchrotron radiation experiment was performed at BL02B2 of SPring-8 with the approval of JASRI (Proposals 2011A1492, 2011B1906, and 2012A1690).

■ REFERENCES

(1) Novoselov, K. S.; Geim, A. K.; Morozov, S. V.; Jiang, D.; Zhang, Y.; Dubonos, S. V.; Grigorieva, I. V.; Firsov, A. A. *Science* **2004**, *306*, 666.
(2) Geim, A. K.; Novoselov, K. S. *Nat. Mater.* **2007**, *6*, 183.
(3) Lin, Y.-M.; Dimitrakopoulos, C.; Jenkins, K. A.; Farmer, D. B.; Chiu, H.-Y.; Grill, A.; Avouris, Ph. *Science* **2010**, *327*, 662.
(4) Bonaccorso, F.; Sun, Z.; Hasan, T.; Ferrari, A. C. *Nat. Photonics* **2010**, *4*, 611.
(5) Son, Y.-W.; Cohen, M. L.; Louie, S. G. *Nature* **2006**, *444*, 347.
(6) Maassen, J.; Ji, W.; Guo, H. *Nano Lett.* **2011**, *11*, 151.
(7) Sasaki, T.; Watanabe, M.; Hashizume, H.; Yamada, H.; Nakagawa, H. *J. Am. Chem. Soc.* **1996**, *118*, 8329.
(8) Li, B.-W.; Osada, M.; Ozawa, T. C.; Ebina, Y.; Akatsuka, K.; Ma, R.; Funakubo, H.; Sasaki, T. *ACS Nano* **2010**, *4*, 6673.
(9) Umar, A.; Hahn, Y. B. *Nanotechnology* **2006**, *17*, 2174.
(10) Sakai, N.; Ebina, Y.; Takada, K.; Sasaki, T. *J. Am. Chem. Soc.* **2004**, *126*, 5851.
(11) Muramatu, M.; Akatsuka, K.; Ebina, Y.; Wang, K.; Sasaki, T.; Ishida, T.; Miyake, K.; Haga, M. *Langmuir* **2005**, *21*, 6590.
(12) Coleman, J. N.; et al. *Science* **2011**, *331*, 568.
(13) Splendiani, A.; Sun, L.; Zhang, Y.; Li, T.; Kim, J.; Chim, C.-Y.; Galli, G.; Wang, F. *Nano Lett.* **2010**, *10*, 1271.
(14) Lee, H. S.; Min, S.-W.; Park, M. K.; Lee, Y. T.; Jeon, P. J.; Kim, J. H.; Ryu, S.; Im, S. *Small* **2012**, *8*, 3111.
(15) Zeng, Z.; Yin, Z.; Huang, X.; Li, H.; He, Q.; Lu, G.; Boey, F.; Zhang, H. *Angew. Chem., Int. Ed.* **2011**, *50*, 11093.
(16) Ma, R.; Liu, Z.; Li, L.; Iyi, N.; Sasaki, T. *J. Mater. Chem.* **2006**, *16*, 3809.
(17) Ma, R.; Liu, Z.; Takada, K.; Iyi, N.; Bando, Y.; Sasaki, T. *J. Am. Chem. Soc.* **2007**, *129*, 5257.
(18) Ida, S.; Shiga, D.; Koinuma, M.; Matsumoto, Y. *J. Am. Chem. Soc.* **2008**, *130*, 14038.
(19) Yan, D.; Lu, J.; Wei, M.; Han, J.; Ma, J.; Li, F.; Evans, D. G.; Duan, X. *Angew. Chem., Int. Ed.* **2009**, *48*, 3073.
(20) Yan, D.; Lu, J.; Ma, J.; Wei, M.; Evans, D. G.; Duan, X. *Angew. Chem., Int. Ed.* **2011**, *50*, 720.
(21) Okamoto, H.; Kumai, Y.; Sugiyama, Y.; Mitsuoka, T.; Nakanishi, K.; Ohta, T.; Nozaki, H.; Yamaguchi, S.; Shirai, S.; Nakano, H. *J. Am. Chem. Soc.* **2010**, *132*, 2710.
(22) Kim, U.; Kim, I.; Park, Y.; Lee, K.-Y.; Yim, S.-Y.; Park, J.-G.; Ahn, H.-G.; Park, S.-H.; Choi, H.-J. *ACS Nano* **2011**, *5*, 2176.
(23) Lu, Z.; Zhu, J.; Sim, D.; Zhou, W.; Shi, W.; Hng, H. H.; Yan, Q. *Chem. Mater.* **2011**, *23*, 5293.
(24) Makiura, R.; Motoyama, S.; Umemura, Y.; Yamanaka, H.; Sakata, O.; Kitagawa, H. *Nat. Mater.* **2010**, *9*, 565.
(25) Colson, J. W.; Woll, A. R.; Mukherjee, A.; Levendorf, M. P.; Spitler, E. L.; Shields, V. B.; Spencer, M. G.; Park, J.; Dichtel, W. R. *Science* **2011**, *332*, 228.
(26) Spitler, E. L.; Koo, B. T.; Novotney, J. L.; Colson, J. W.; Uribe-Romo, F. J.; Gutierrez, G. D.; Clancy, P.; Dichtel, W. R. *J. Am. Chem. Soc.* **2011**, *133*, 19416.
(27) Bauer, T.; Zheng, Z.; Renn, A.; Enning, R.; Stemmer, A.; Sakamoto, J.; Schlüter, A. D. *Angew. Chem., Int. Ed.* **2011**, *50*, 7879.
(28) Schrauzer, G. N. *Acc. Chem. Res.* **1969**, *2*, 72.
(29) Nishihara, H.; Okuno, M.; Kogawa, N.; Aramaki, K. *J. Chem. Soc., Dalton Trans.* **1998**, 2651.
(30) Shibata, Y.; Zhu, B.-H.; Kume, S.; Nishihara, H. *Dalton Trans.* **2009**, 1939.
(31) Kambe, T.; Tsukada, S.; Sakamoto, R.; Nishihara, H. *Inorg. Chem.* **2011**, *50*, 6856.
(32) Cassoux, P. *Coord. Chem. Rev.* **1999**, *185−186*, 213.
(33) Kato, R. *Chem. Rev.* **2004**, *104*, 5319.
(34) Ray, K.; Weyhermüller, T.; Neese, F.; Wieghardt, K. *Inorg. Chem.* **2005**, *44*, 5345.
(35) Sellmann, D.; Binder, H.; Häußinger, D.; Heinemann, F. W. *Inorg. Chim. Acta* **2000**, *300−302*, 829.
(36) Connelly, N. G.; Geiger, W. E. *Chem. Rev.* **1996**, *96*, 877.
(37) Gupta, A.; Chen, G.; Joshi, P.; Tadigadapa, S.; Eklund, P. C. *Nano Lett.* **2006**, *6*, 2667.